

Supplementary Information

Oxygen vacancy assisted Ru-Ni(OH)₂ for efficient ethylene glycol electrooxidation reaction

Yanyan Li^a, Xiaobin Liu^{a,b*}, Ketao Wang^a, Jingqi Chi^a, Haifeng Lin^a, Lei Wang^{a*}

^a State Key Laboratory Base of Eco-Chemical Engineering, International Science and Technology Cooperation Base of Eco-chemical Engineering and Green Manufacturing, College of Chemistry and Molecular Engineering, Qingdao University of Science and Technology, Qingdao 266042, PR China.

^b College of Environment and Safety Engineering, Qingdao University of Science and Technology, Qingdao 266042, P.R. China.

1. Experimental section

1.1 Experimental material

Ruthenium (III) chloride (RuCl_3), sodium hydrosulfide (NaHS) and potassium hydroxide (KOH) were purchased from Shanghai Aladdin Biochemical Technology Co., Ltd. Sodium chloride (NaCl), ethanol, ethylene glycol and acetone were purchased from Sinopharm Chemical Reagent Co., Ltd. Nickel foam (NF, 99.8 wt %, 1.0 mm in thickness) was purchased in Suzhou Kesheng and Metal Materials. All reagents received were used without further purification.

1.2. Pre-treatment of nickel foam

The NF was ultrasound, treated in acetone, deionized water and ethanol for 15 min, respectively, and dried in a vacuum oven.

1.3. Product detection

The reaction products were analyzed by a 500 MHz liquid nuclear magnetic resonance spectrometer, Bruker/AVAN CE NEO 500, in which 300 μL electrolyte was added 300 μL D_2O with 30 μL dimethyl sulfoxide used as an internal standard.

1.4. Characterization

Materials characterization: XRD measurement was performed using X'Pert PRO MPD and the scan speed was 5°min^{-1} . Scanning electron microscope (SEM) was used for the characterization by Hitachi S-8200. Transmission electron microscopy (TEM) and high-resolution transmission electron microscopy (HRTEM) were used for the characterization by JEM2100UHR. The vacancy of phosphorus was determined by electron paramagnetic resonance (EPR) spectroscopy, model Bruker A300 Germany. Using X-ray photoelectron spectroscopy (XPS) with a monochromatic aluminum K_α source, chemical valences and atomic compositions were determined. The XPS is calibrated with a C 1s spectrum, where the main line is 284.6 eV.

1.5. Electrochemical testing

Electrochemical measurement: The Gamry Reference 3000 electrochemical workstation was used for electrochemical analyses. The counter electrode was a graphite rod, and the reference electrode was Hg/HgO electrode. The reversible hydrogen electrode's relevant potential for this experiment was determined using the following equation: $E_{\text{RHE}} = E_{\text{Hg}/\text{HgO}} + (0.098 + 0.059 \text{ pH}) \text{ V}$. In solutions containing 1.0 M KOH, 1.0 M KOH + 0.5 M EG, EGOR experiments was conducted. At a scan rate of 5 mV s^{-1} , polarization curves for OER was measured utilizing linear scan

voltammetry without IR compensation. In the frequency between 0.01 to 100 Hz, electrochemical impedance spectroscopy measurements were made. Using CV cycling at various scan speeds (40 - 120 mV s⁻¹), the electrochemically active surface area was determined. Chronoamperometry u-t tests was used to test the long-term stability of the system at 25 °C. The immersion area of the electrode is 1 cm × 1 cm.

2. Results and discussion



Figure S1. Optical images of the as-prepared electrodes.

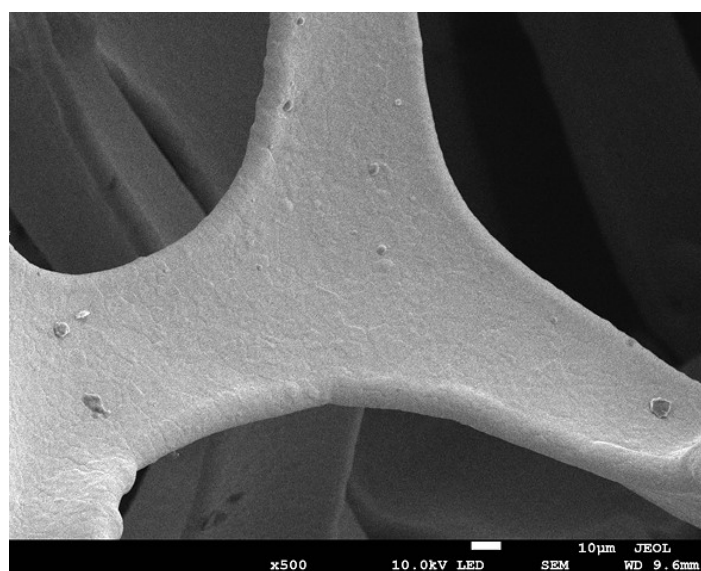


Figure S2. The SEM image of NF.

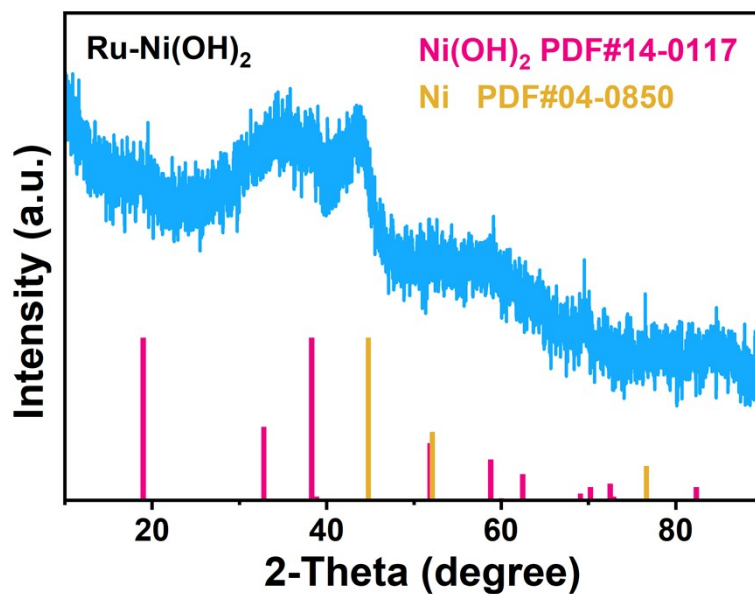


Figure S3. XRD pattern of Ru-Ni(OH)₂.

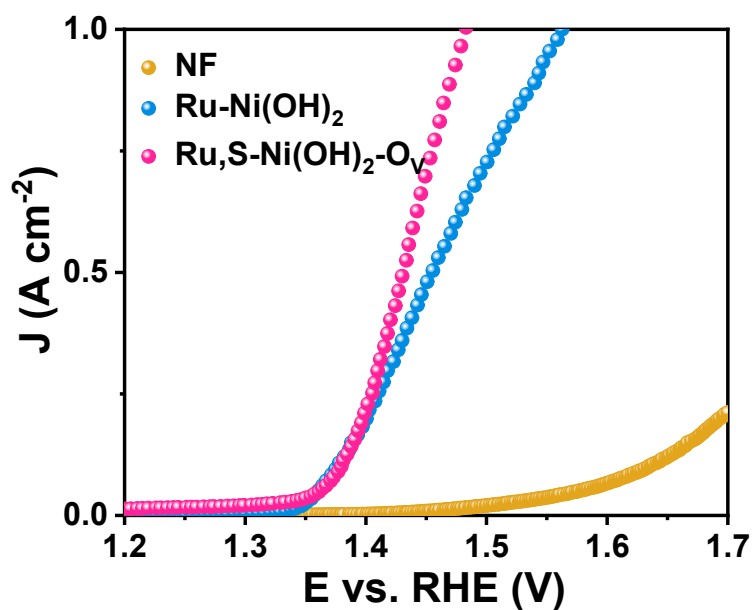


Figure S4. LSV curves of NF, Ru-Ni(OH)₂ and Ru,S-Ni(OH)₂-O_V in 1.0 M KOH + 0.5 M EG solution.

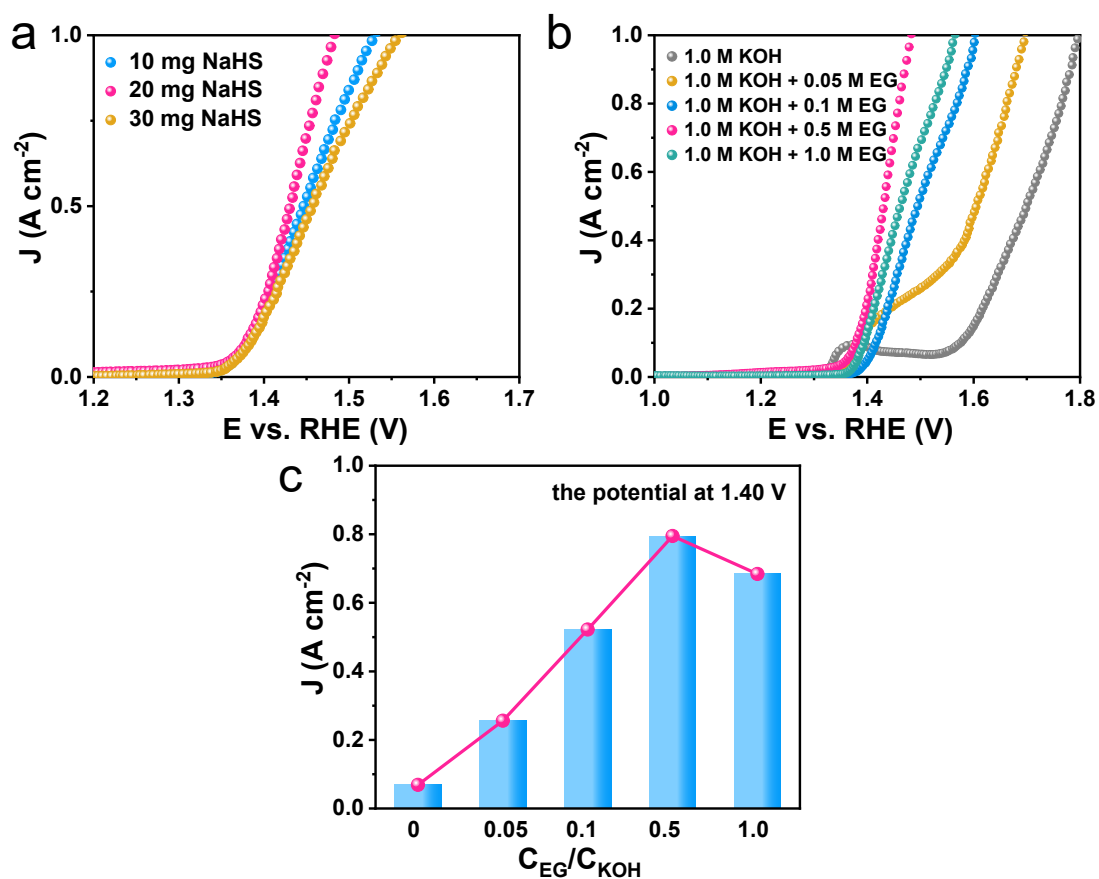


Figure S5. LSV curves for (a) the exploration of optimal S doping content, (b) different EG concentrations, and (c) comparison of current density for different ethylene glycol concentrations at the potential of 1.40 V.

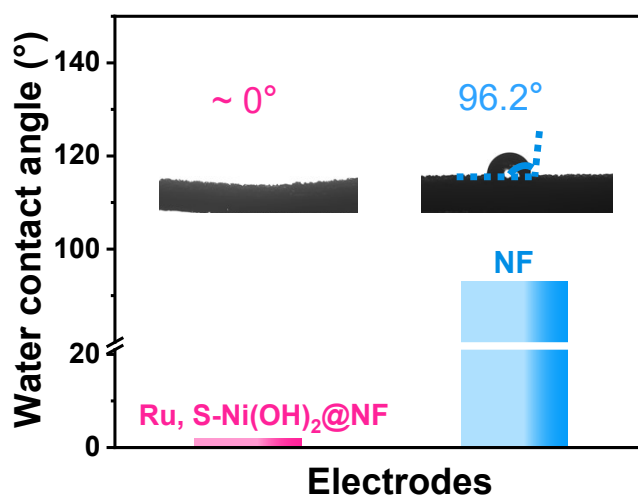


Figure S6. Water contact angles test of the Ru,S-Ni(OH)₂-O_V and NF electrodes.

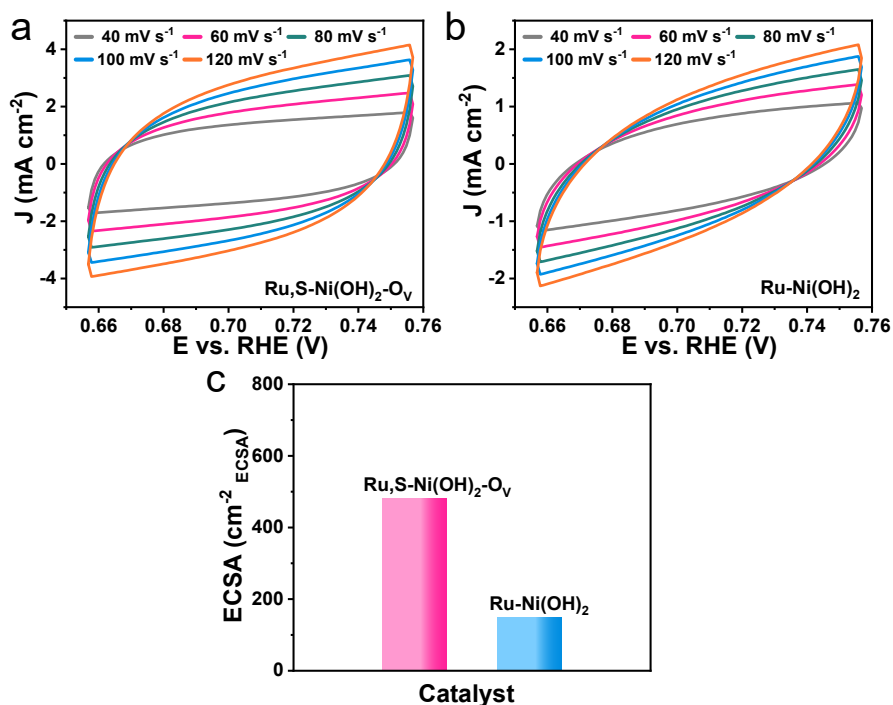


Figure S7. (a-b) The cyclic voltammety curves, (c) the ECSA of Ru-Ni(OH)₂ and Ru,S-Ni(OH)₂-O_v in the non-Faradaic region.

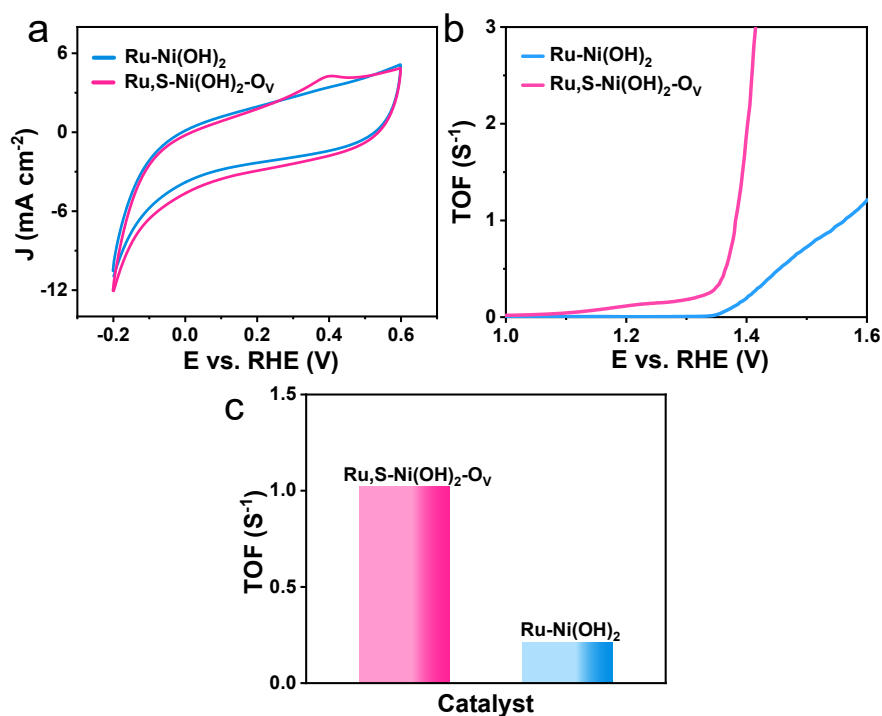


Figure S8. (a) CV curves for recorded between -0.2 V and 0.6 V vs. RHE in 1.0 M PBS (pH = 7) at a scan rate of 50 mV s⁻¹, (b) TOFs of Ru-Ni(OH)₂ and Ru,S-Ni(OH)₂-O_v, (c) TOFs of Ru-Ni(OH)₂ and Ru,S-Ni(OH)₂-O_v at the potential of 1.42 V vs. RHE.

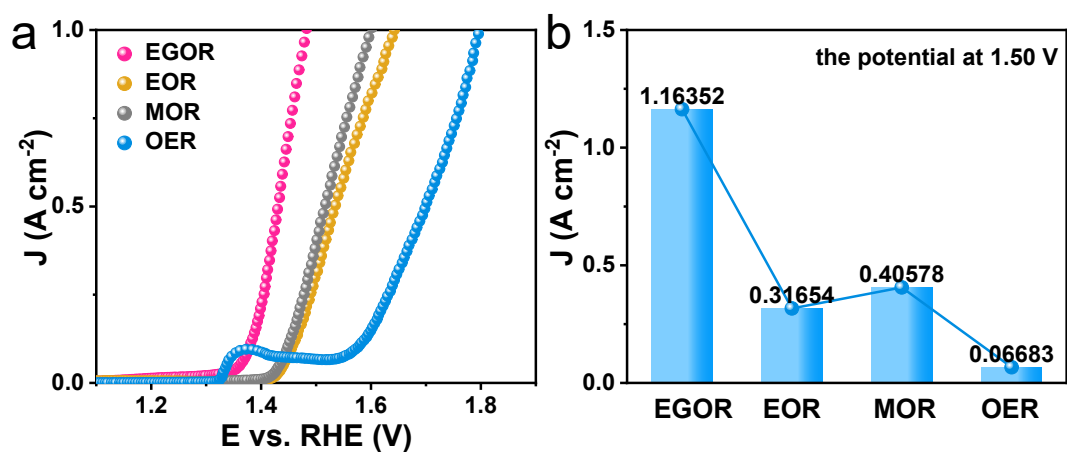


Figure S9. (a) Comparison of catalytic activity of Ru,S-Ni(OH)₂-O_V electrodes in methanol, ethanol and ethylene glycol alkaline solutions, and (b) comparison of current density at 1.50 V potential at different alkaline alcohol solutions.

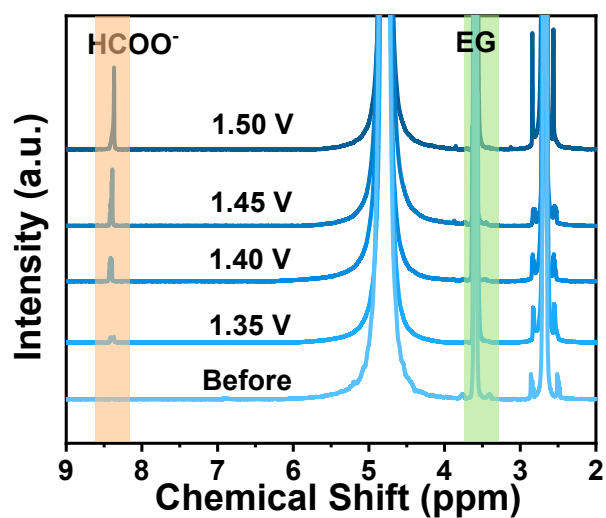


Figure S10. The ¹H NMR spectrum of Ru,S-Ni(OH)₂-O_V at the applied potential.

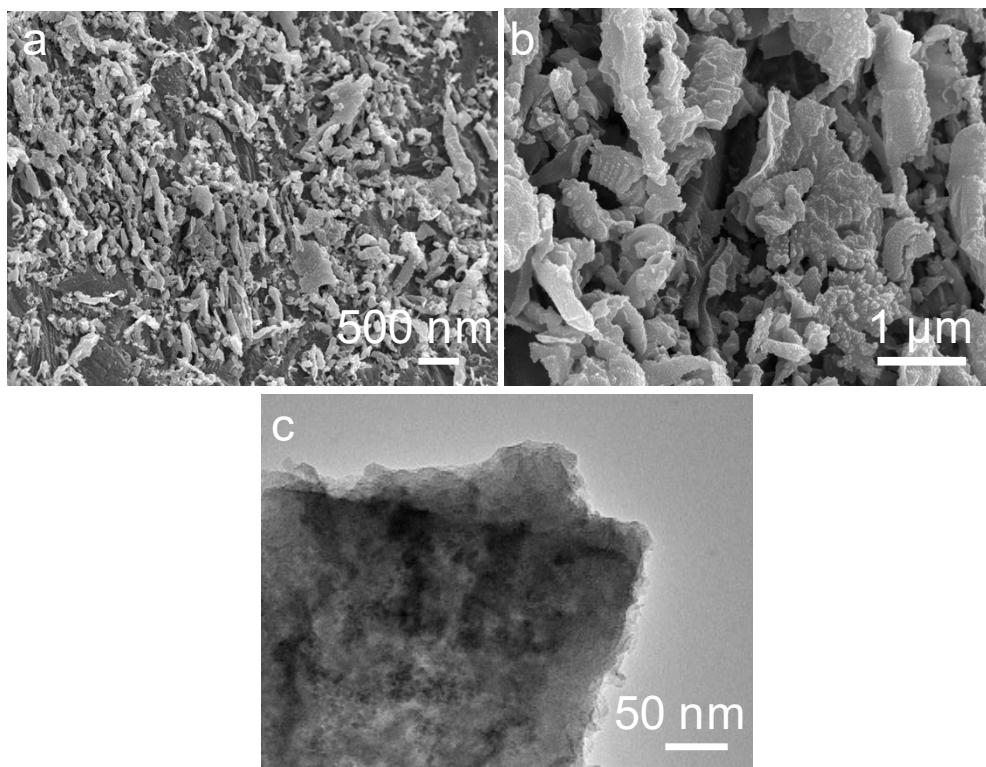


Figure S11. (a-b) SEM and (c) TEM images after EGOR stability test.

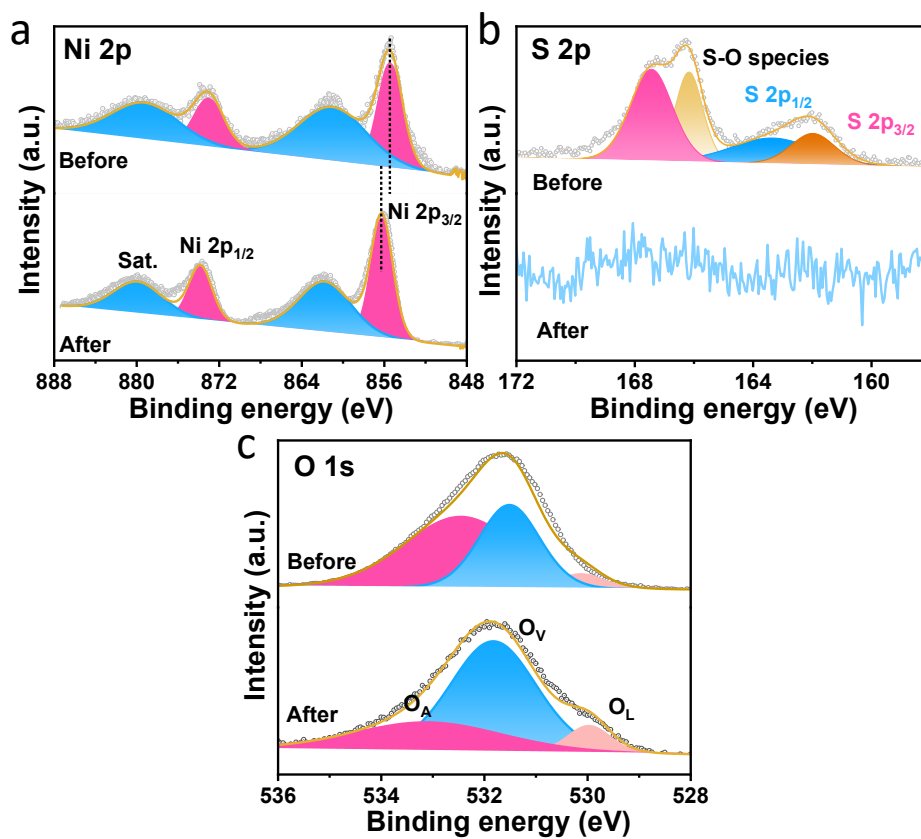


Figure S12. (a) High-resolution XPS of (a) Ni 2p, (b) S 2p and (c) O 1s before and after the reaction of Ru,S-Ni(OH)₂-O_v.

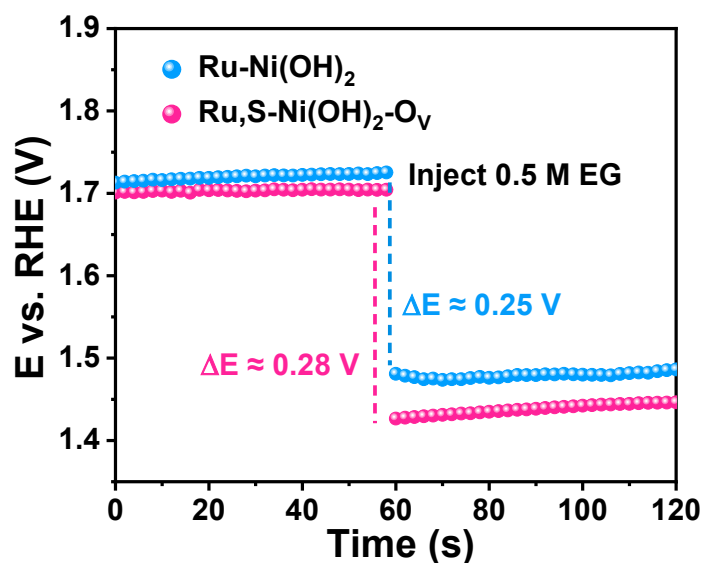


Figure S13. Potential of Ru-Ni(OH)₂ and Ru,S-Ni(OH)₂-O_v when injected with EG.

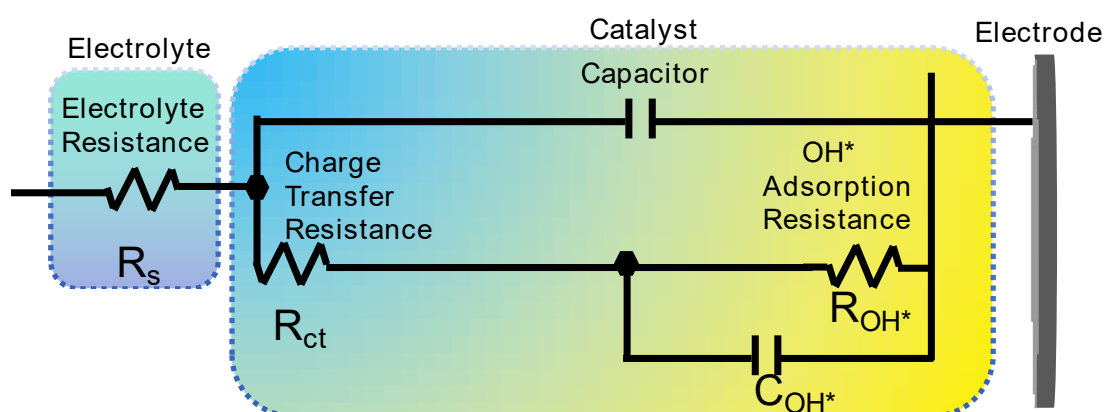


Figure S14. Equivalent circuit model used in the fitting of the impedance data.

R_s represents solution impedance, R_{ct} represents interfacial charge transfer impedance, and C represents non-ideal capacitance to fit the double layer capacitance (C_{dl}). The non-ideal bilayer behavior mainly comes from the adsorption of OH* in the diffusion bilayer (DDL) region. The variance of OH* is defined as C_φ , the absorption coverage of OH* in the reaction is analyzed, and R_{OH^*} is the corresponding hydroxyl adsorption impedance.

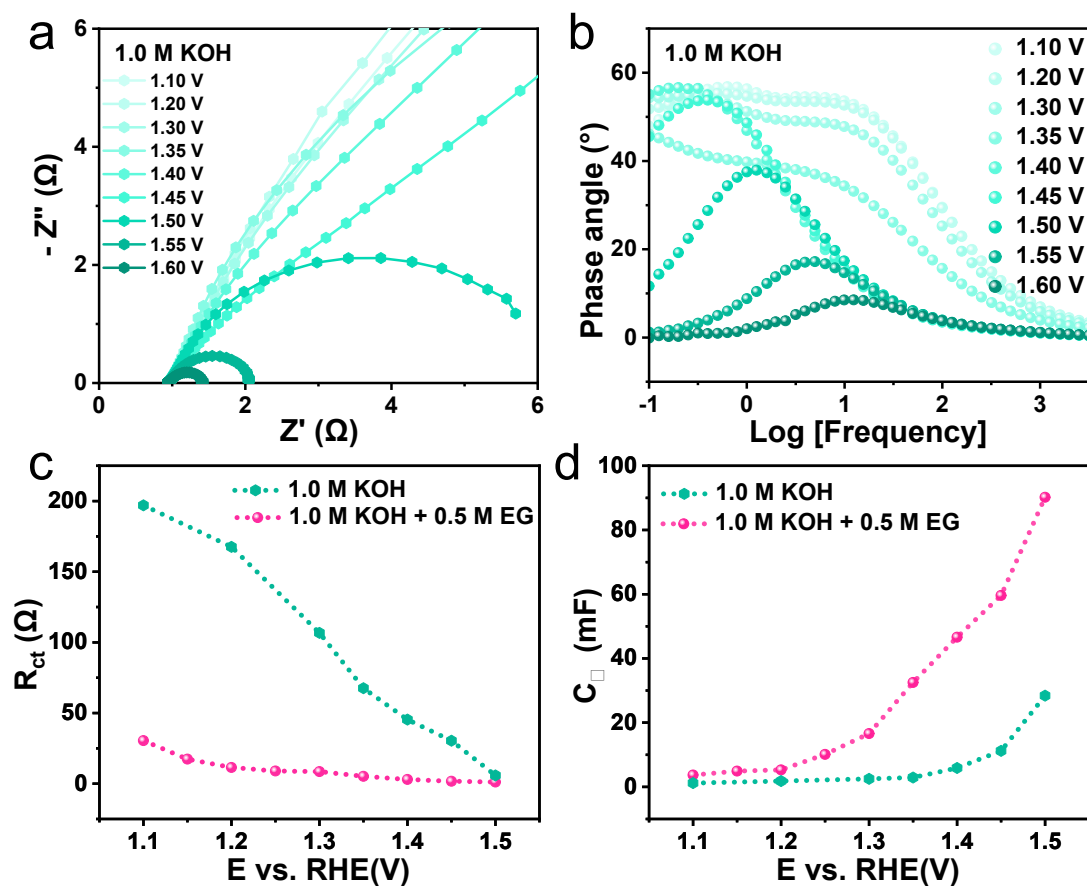


Figure S15. Operando electrochemical impedance spectra on Ru,S-Ni(OH)₂-O_V electrode at different potentials in (a) 1.0 M KOH and (b) the corresponding Bode phase plots on Ru,S-Ni(OH)₂-O_V electrode during OER, plot of (c) charge transfer resistance plot and (d) CPE_{OH} versus to the applied potential of Ru,S-Ni(OH)₂-O_V electrode.

Table S1 Comparison of the EGOR activities of Ru,S-Ni(OH)₂-O_V with recently reported electrocatalysts.

Catalysts	Electrolytes	Current density (mA cm ⁻²)	Potential (mV)	Reference
Ru,S-Ni(OH) ₂ -O _V	1.0 M KOH + 0.5	50	1.35	This work
	M EG	100	1.36	
nanoNi-Pop (CV)	1.0 M KOH + 0.1	50	1.56	1
	M EG			
NiO@C/CC	1.0 M KOH + 1.0	50	1.66	2
	M EG	100	1.82	
NiCo ₂ O ₄ /CFP	1.0 M NaOH +	50	1.43	3
	0.06 M EG	100	1.47	
CuCo ₂ O ₄ /NF	1.0 M KOH + 0.06	50	1.36	4
	M EG	100	1.47	
Ni/WC@C	1.0 M NaOH + 1 M	50	1.40	5
	EG	100	1.45	
OMS-Ni ₁ -CoP	1.0 M KOH + 0.5	50	1.38	6
	M EG	100	1.42	
Bi _{0.13} Co _{2.83} O ₄ -550	1.0 M KOH + 1.0	50	1.39	7
	M EG	100	1.42	
Ni ₃ N- Ni _{0.2} M _{0.8} NNWs/C	1.0 M KOH + 0.3	50	1.38	8
	M EG	100	1.43	
rGO-NiMn	1.0 M KOH + 1 M	~47.5	1.49	9
	EG			
Ni-Co Oxides	1.0 M KOH + 1.0	~55	1.49	10
	M EG			
Fe-Co-Ni/C	0.5 M KOH + 1.0	~38.5	1.50	11
	M EG			

Branched NiSe ₂ /C	1.0 M KOH + 1.0 M EG	~103.6	1.60	12
-------------------------------	-------------------------	--------	------	----

Reference

1. C.-Y. Lin, S.-C. Huang, Y.-G. Lin, L.-C. Hsu and C.-T. Yi, Electrosynthesized Ni-P nanospheres with high activity and selectivity towards photoelectrochemical plastics reforming, *Appl. Catal. B Environ.*, 2021, **296**, 120351.
2. C. Liu, W. Zhou, J. Zhang, Z. Chen, S. Liu, Y. Zhang, J. Yang, L. Xu, W. Hu, Y. Chen and Y. Deng, Air-assisted transient synthesis of metastable nickel oxide boosting alkaline fuel oxidation reaction, *Adv. Energy Mater.*, 2020, **10**, 2001397.
3. J. Wang, X. Li, M. Wang, T. Zhang, X. Chai, J. Lu, T. Wang, Y. Zhao and D. Ma, Electrocatalytic valorization of poly (ethylene terephthalate) plastic and CO₂ for simultaneous production of formic acid, *ACS Catal.*, 2022, **12**, 6722-6728.
4. F. Liu, X. Gao, R. Shi, E. C. M. Tse and Y. A general electrochemical strategy for upcycling polyester plastics into added-value chemicals by a CuCo₂O₄ catalyst, *Chem. Green Chem.*, 2022, **24**, 6571-6577.
5. M. Zhang, J. Zhu, R. Wan, B. Liu, D. Zhang, C. Zhang, J. Wang and J. Niu, Synergistic effect of nickel oxyhydroxide and tungsten carbide in electrocatalytic alcohol oxidation, *Chem. Mater.* 2022, **34**, 959-969.
6. N. Wang, X. Li, M.-K. Hu, W. Wei, S.-H. Zhou, X.-T. Wu and Q.-L. Zhu, Ordered macroporous superstructure of bifunctional cobalt phosphide with heteroatomic modification for paired hydrogen production and polyethylene terephthalate plastic recycling, *Appl. Catal. B Environ.*, 2022, **316**, 121667.
7. F. Zhao, B. Zhu, S. Li, X. Kong and Q. Liu, J. Taiwan Inst. Bismuth-doped cobaltic oxide as a noble-metal free electrocatalyst for the efficient methanol oxidation reaction, *Chem. Eng.*, 2022, **131**, 104182.

8. X. Liu, Z. Fang, X. Teng, Y. Niu, S. Gong, W. Chen, T. J. Meyer and Z. Paired formate and H₂ productions via efficient bifunctional Ni-Mo nitride nanowire electrocatalysts, *Chem, J. Energy Chem.*, 2022, **72**, 432-441.
9. M. A. Hefnawy, S. A. Fadlallah, R. M. El-Sherif and S. S. Medany, Nickel-manganese double hydroxide mixed with reduced graphene oxide electrocatalyst for efficient ethylene glycol electrooxidation and hydrogen evolution reaction, *Synth. Met.*, 2021, **282**, 116959.
10. S. Sun, Y. Zhou, B. Hu, Q. Zhang and Z. J. Xu, Ethylene glycol and ethanol oxidation on spinel Ni-Co oxides in alkaline, *J Electrochem. Soc.*, 2015, **163**, H99-H104.
11. A. Gayathri, S. Kiruthika, V. Selvarani, M. S. AlSalhi, S. Devanesan, W. Kim and B. Muthukumar, Evaluation of iron-based alloy nanocatalysts for the electrooxidation of ethylene glycol in membraneless fuel cells, *Fuel*, 2022, **321**, 124059.
12. J. Li, L. Li, X. Ma, X. Han, C. Xing, X. Qi, R. He, J. Arbiol, H. Pan, J. Zhao, J. Deng, Y. Zhang, Y. Yang and A. Cabot, Selective ethylene glycol oxidation to formate on nickel selenide with simultaneous evolution of hydrogen, *Adv. Sci.* 2023, **10**, 2300841.